JOURNAL OF GEOPHYSICAL RESEARCH, VOL. 114, D00D14, doi:10.1029/2008JD010975, 2009

Variations of meridional aerosol distribution and solar dimming

P. Kishcha,[1] B. Starobinets,[1] O. Kalashnikova,[2] C. N. Long,[3] and P. Alpert[1]

Received 12 August 2008; revised 19 February 2009; accepted 25 February 2009; published 22 May 2009.

[1] Meridional distribution of aerosol optical thickness (AOT) over the ocean was analyzed by using the 8-year MISR and MODIS-Terra data sets from March 2000 to February 2008, as well as the 5-year MODIS-Aqua data set from July 2002 to June 2007. The three satellite sensors show that there was a pronounced meridional aerosol asymmetry. It was found that there were strong seasonal variations in the meridional aerosol asymmetry: it was most pronounced in the April–July months. There was no noticeable asymmetry during the season from September to December. The Northern Hemisphere, where the main sources of natural and anthropogenic aerosols are located, contributed to the formation of noticeable aerosol asymmetry. During the season of pronounced hemispheric aerosol asymmetry, an increase in AOT was observed over the Northern Hemisphere, while a decrease in AOT was observed over the Southern Hemisphere. At midlatitudes in the Northern Hemisphere (30–60°N), the main contribution to seasonal variations of AOT over the ocean was made by Pacific Ocean aerosols. At low latitudes in the Northern Hemisphere (0–30°N), aerosols over the Atlantic Ocean contributed to seasonal variations of AOT more significantly than aerosols over the Pacific Ocean. During the 8-year period under consideration, the brightening phenomenon, detected over the land, was not observed over the ocean at midlatitudes 30–60°N in cloudless conditions.

Citation: Kishcha, P., B. Starobinets, O. Kalashnikova, C. N. Long, and P. Alpert (2009), Variations of meridional aerosol distribution and solar dimming, *J. Geophys. Res.*, *114*, D00D14, doi:10.1029/2008JD010975.

1. Introduction

[2] Atmospheric aerosols and clouds are two main factors which modulate the solar radiation flux reaching the Earth's surface. This means they play an important role in the reported changes in solar radiation at the Earth's surface: known as the dimming-brightening phenomenon [*Stanhill and Cohen*, 2001; *Liepert*, 2002; *Wild et al.*, 2005; *Pinker et al.*, 2005; *Alpert et al.*, 2005; *Alpert and Kishcha*, 2008]. Considerable recent attention has been focused on the direct effect of aerosols on the modulation of surface solar radiation [*Romanou et al.*, 2007; *Ramanathan et al.*, 2007]. In cloudless conditions, aerosol trends could account for most of the solar dimming-brightening. To quantify the aerosol effects on the modulation of surface solar radiation, a detailed knowledge of aerosol distributions in space and time is necessary.

[3] Unlike ground-based measurements, satellite remote sensing of aerosols has the advantage of providing global coverage on a regular basis [*Kaufman et al.*, 2002; *Mishchenko et al.*, 2007]. This provides us with an opportunity to estimate space and time distributions of aerosol radiative properties over the entire globe, albeit with less uncertainty over the ocean than over the land. The space distribution of aerosol optical thickness has been analyzed in several previous studies, using satellite data. These studies show that the hemispheres are asymmetric in aerosol parameters. *Mishchenko and Geogdzhayev* [2007] used the Advanced Very High Resolution Radiometer (AVHRR) satellite data over the ocean, from August 1981 to June 2005, to compare monthly averaged aerosol optical thickness (AOT) over the Northern Hemisphere and that over the Southern Hemisphere. They found a difference in AOT averaged over the hemispheres. *Chou et al.* [2002] obtained meridional distribution of AOT over the ocean by using SeaWIFS satellite data at 0.865 μm for the year of 1998. The phenomenon of hemispheric asymmetry in AOT was displayed in several previous studies based on the Moderate Resolution Imaging Spectroradiometer (MODIS) data [*Remer et al.*, 2005, 2008; *Kaufman et al.*, 2005a; *Remer and Kaufman*, 2006]. In the aforementioned studies global maps were presented, which showed an essential difference of AOT between the two hemispheres. However, variations of meridional distribution of AOT were not analyzed in detail. As recently obtained by *Kishcha et al.* [2007], collection 4 of MODIS data indicated a pronounced hemispheric asymmetry in meridional variations of AOT, on a global scale. In contrast to AOT, cloud optical thickness was found to be quite symmetrical in both hemispheres.

[1]Department of Geophysics and Planetary Sciences, Tel Aviv University, Tel Aviv, Israel.
[2]Jet Propulsion Laboratory, California Institute of Technology, Pasadena, California, USA.
[3]Pacific Northwest National Laboratory, Richland, Washington, USA.

0148-0227/09/2008JD010975$09.00

Table 1. Average AOT/FAOT/CF Over the Northern (X_N) and Southern (X_S) Hemispheres and their Hemispheric Ratio (R)[a]

	AOT			FAOT			CF	
		MODIS			MODIS		MODIS	
	MISR	Terra	Aqua	MISR	Terra	Aqua	Terra	Aqua
$X_N \pm \sigma_N$	0.21 ± 0.03	0.20 ± 0.04	0.19 ± 0.04	0.08 ± 0.02	0.11 ± 0.03	0.10 ± 0.02	0.70 ± 0.02	0.71 ± 0.02
$X_S \pm \sigma_S$	0.15 ± 0.02	0.14 ± 0.02	0.13 ± 0.02	0.06 ± 0.02	0.06 ± 0.02	0.06 ± 0.01	0.71 ± 0.01	0.71 ± 0.01
$R \pm \sigma_R$	1.39 ± 0.03	1.46 ± 0.04	1.51 ± 0.05	1.34 ± 0.05	1.67 ± 0.06	1.74 ± 0.07	0.98 ± 0.01	1.00 ± 0.01

[a]Standard deviations of X_N, X_S, and R are designated by σ_N, σ_S, and σ_R, respectively. Eight-year MISR and MODIS-Terra data sets and the 5-year MODIS-Aqua data set over the global ocean (180°W to180°E, 60°N to 60°S) were used. AOT, aerosol optical thickness; FAOT, fine aerosol optical thickness; CF, cloud fraction.

[4] An analysis of meridional distribution of aerosol radiative properties and its tendency is of importance to our understanding of the solar dimming and brightening phenomenon within different latitudinal zones. The current study was aimed at conducting such an analysis of meridional aerosol distribution, its seasonal variations, and long-term tendencies, by using 8-year data sets of Multiangle Imaging SpectroRadiometer (MISR) and MODIS sensors onboard the NASA Terra satellite. In addition, we used the 5-year data set of another MODIS sensor onboard the NASA Aqua satellite, which also provides information about the meridional aerosol distributions. The data sets used include Level-3 gridded monthly data of total aerosol optical thickness (AOT) and fine aerosol optical thickness (FAOT) at 550 nm. The large volume of data enables examination of the spatial and temporal variability in meridional distribution of aerosol properties.

[5] Note that in the current study, meridional aerosol distributions were analyzed only over the ocean, where satellite aerosol retrievals are more accurate than over the land [*Remer et al.*, 2005; *Levy et al.*, 2007a]. Over the ocean, the solar dimming phenomenon could not be analyzed during the presatellite period because of the lack of long-term regular radiation measurements. Changes in atmospheric aerosols could be usefully obtained by satellite aerosol retrievals. Some estimates of the AOT trends over the global ocean and specific regions were obtained in previous studies based on AVHRR data sets [*Zhao et al.*, 2008; *Mishchenko et al.*, 2007; *Mishchenko and Geogdzhayev*, 2007] and also on MODIS-Terra data [*Remer et al.*, 2008; *Papadimas et al.*, 2008a, 2008b].

[6] In the current study, meridional distributions of aerosol optical thickness were verified by comparing the three sensors. MODIS has a wide viewing swath and its cameras are focused strait down relative to the Earth's surface. MISR is a multiangle imaging instrument: its cameras acquire images with several angles relative to the Earth's surface [*Diner et al.*, 1998]. The multiangle views ensure that MISR can provide aerosol optical thickness retrievals in areas where Sun's glint precludes MODIS from doing so. MISR and MODIS aerosol retrievals successfully compliment each other [*Kalashnikova and Kahn*, 2009]. Furthermore, the MISR and MODIS data sets are the most compatible ones in terms of their duration, spatial resolution, and spatial, temporal, and spectral overlap as well as of their retrieval approaches [*Mishchenko et al.*, 2007]. Therefore, comparisons between aerosol optical thickness and its tendencies based on MISR data and those based on MODIS data can help us expand our knowledge about ocean aerosols.

2. Data and Methodology

[7] The present study used Level-3 monthly gridded aerosol data with horizontal resolution $1° \times 1°$ from the three sensors: MISR, MODIS-Terra, and MODIS-Aqua. MISR and MODIS-Terra are onboard the NASA Terra spacecraft orbiting the Earth since December 1999, with daytime equator crossing at 1030 LT. MODIS-Aqua is another MODIS sensor onboard the NASA Aqua spacecraft launched in May 2002, with daytime equator crossing at 0130 LT.

[8] To obtain meridional aerosol distribution, two main aerosol products were used: total aerosol optical thickness (AOT) and fine aerosol optical thickness (FAOT) attributed to submicron particles. Variations of meridional aerosol distributions were analyzed by using MISR and MODIS-Terra retrievals during the 8-year period, from March 2000 to February 2008, supplemented by the 5-year MODIS-Aqua data, from July 2002 to June 2007.

[9] MODIS with its 2330 km viewing swath provides almost daily global coverage. Collection 5 (MOD08_M3-005) of MODIS data were used which is considered to be of a better quality than collection 4 [*Levy et al.*, 2007a; *Jethva et al.*, 2007; *Papadimas et al.*, 2008b]. The MODIS data were acquired using the GES-DISC Interactive Online Visualization and Analysis Infrastructure (Giovanni) as part of NASA Goddard Earth Sciences (GES) Data and Information Services Center (DISC) [*Acker and Leptoukh*, 2007].

[10] MODIS has separate algorithms for retrieving aerosol products over land and ocean. The MODIS overocean algorithm is more accurate than the overland algorithm [*Remer et al.*, 2005; *Levy et al.*, 2007a]: the AOT uncertainty is ±0.03 ± 0.05 AOT over the ocean and ±0.05 ± 0.15 AOT over the land. The aerosol fine fraction retrieved by MODIS over the ocean is considered reliable [*Bellouin et al.*, 2005]. MODIS aerosol data sets have been validated by using AERONET ground-based instruments both on a global scale [*Chu et al.*, 2002; *Remer et al.*, 2002, 2005; *Kleidman et al.*, 2005] and over different regions [*Ichoku et al.*, 2003; *Levy et al.*, 2003, 2005; *Chu et al.*, 2005]. Besides validating MODIS aerosol products against accurate suborbital measurements, the bias due to cloudiness and assumptions in the retrievals has been analyzed [*Kaufman et al.*, 2005b; *Levy et al.*, 2005; *Remer et al.*, 2005] which has

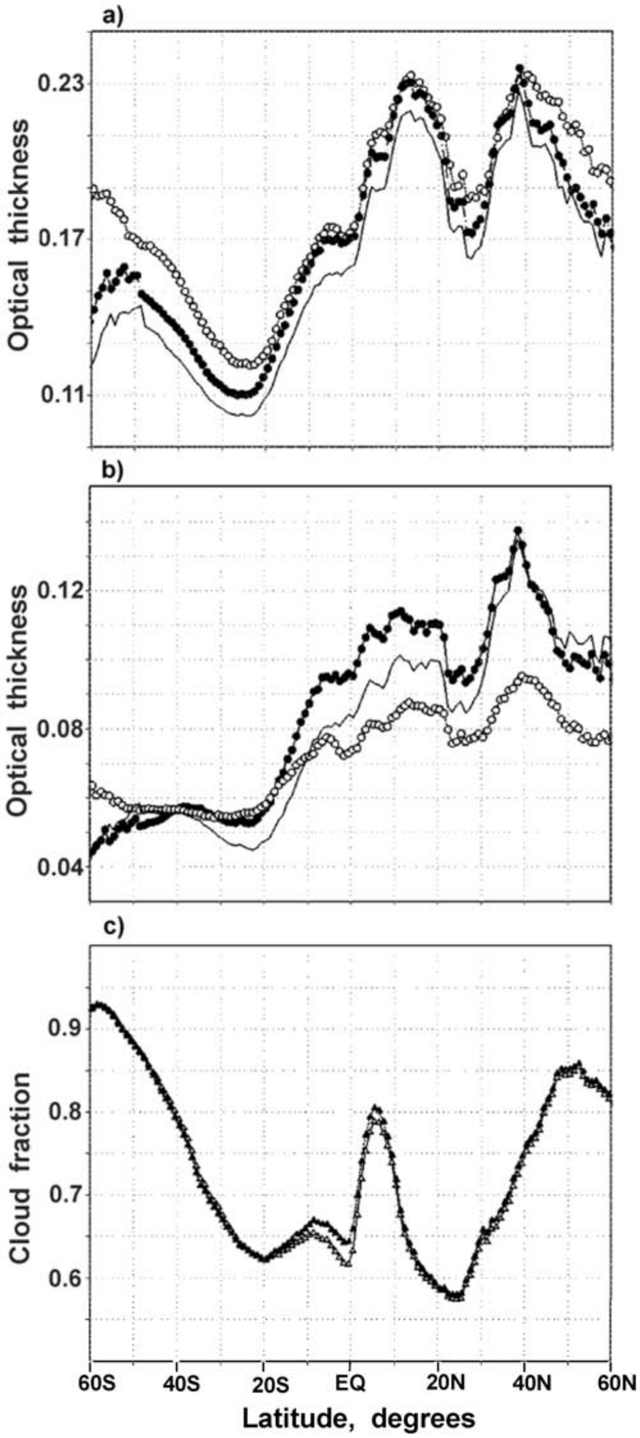

Figure 1. Meridional distribution of (a) total aerosol optical thickness (AOT), (b) fine aerosol optical thickness (FAOT), and (c) cloud fraction, zonally averaged over the global ocean. For AOT/FAOT, the lines with open circles correspond to MISR, the lines with solid circles correspond to MODIS-Terra, and the solid lines with no mark correspond to MODIS-Aqua. For cloud fraction, the line with solid triangles corresponds to MODIS-Terra, and the line with open triangles corresponds to MODIS-Aqua.

been partly mitigated in the collection 5 product [*Levy et al.*, 2007a, 2007b].

[11] MISR is a multiangle (9 view) imaging instrument operating on four spectral bands centered at 446, 558, 672, and 867 nm [*Diner et al.*, 1998]. The fore-aft-nadir cameras acquire images with view angles relative to the Earth's surface: at 0°, 26°, 46°, 60°, and 70°. In its global observing mode, the data in all bands of the nadir cameras and the red band data of all of the off-nadir cameras are downlinked at full spatial resolution, 275 m.

[12] The swath width is about 380 km and global coverage is obtained every 9 days. MISR AOT has been extensively validated against AERONET Sun photometer measurements over different regions [*Martonchik et al.*, 2004; *Christopher and Wang*, 2004; *Kahn et al.*, 2005; *Liu et al.*, 2004]. It was estimated that overall about 2/3 of the MISR-retrieved AOT values fall within ±0.05 or ±0.2·AOT of Aerosol Robotic Network (AERONET) [*Kahn et al.*, 2005]. MISR uses the same algorithm for retrieving its aerosol products over the land and over the ocean. The MISR data were obtained from the NASA Langley Research Center Atmospheric Sciences Data Center.

[13] For the purpose of comparing meridional aerosol distributions with those of clouds, MODIS-Terra and MODIS-Aqua Level 3 global monthly data, collection 5 of cloud fraction (CF), were used [*King et al.*, 2003].

[14] The variations of averaged total AOT and FAOT as a function of latitude provide a way of analyzing their meridional variations. To quantify the meridional asymmetry of AOT, the ratio of averaged AOT over the Northern Hemisphere to that over the Southern Hemisphere was estimated within the latitudinal interval from 60°N to 60°S. Hereafter, the ratio is called 'hemispheric ratio'. The hemispheric ratio is equal to 1 in the case of the two hemispheres holding approximately the same averaged AOT, and the ratio is

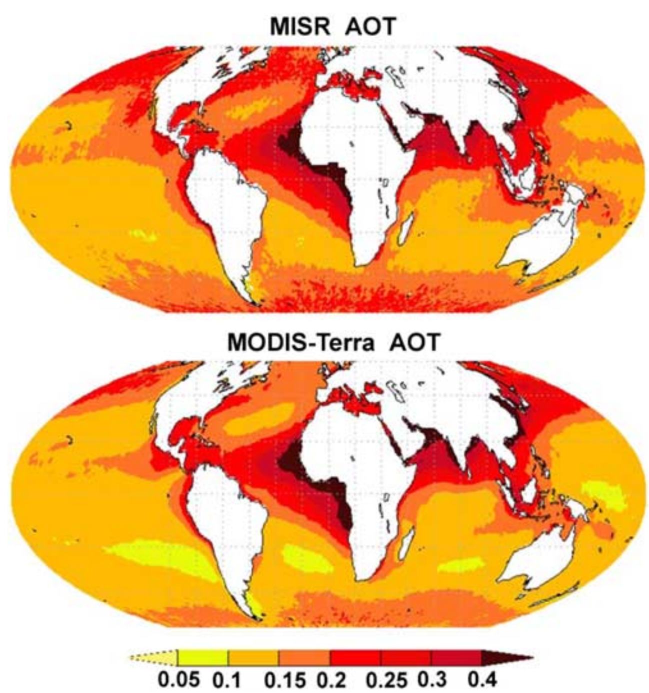

Figure 2. The 8-year mean global distribution of ocean AOT based on (top) MISR and (bottom) MODIS-Terra data sets.

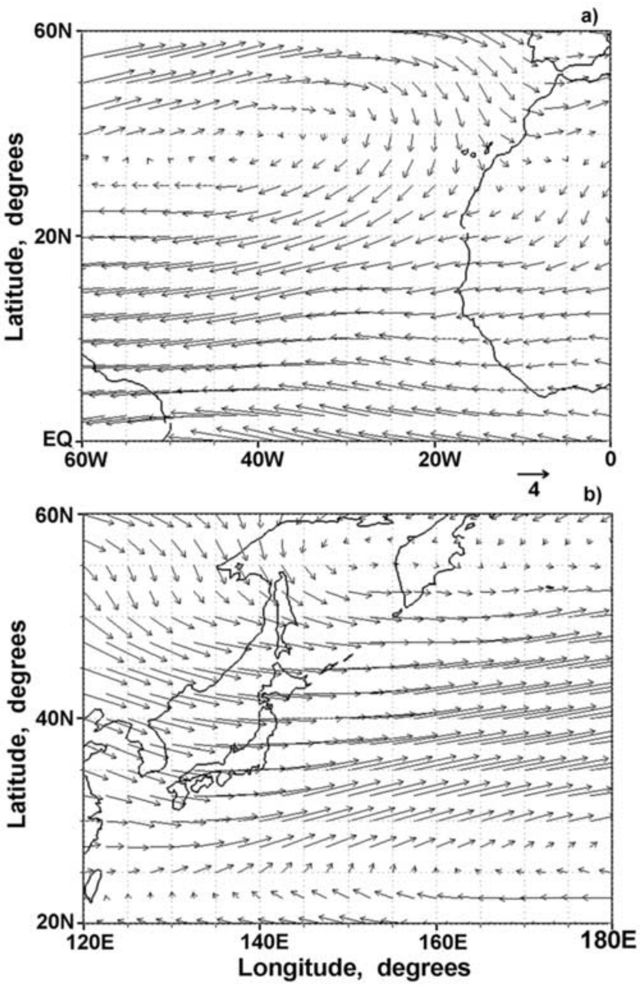

Figure 3. Mean wind vectors of the 700–925 hPa layer averaged over the 8-year period under consideration from March 2000 to February 2008 in the Northern Hemisphere over (a) the Atlantic Ocean (0–40°N; 60°W to 0°E) and (b) the Pacific Ocean (20–60°N; 120–180°E). NCEP/NCAR reanalysis monthly data were used.

greater (less) than 1 if the Northern (Southern) Hemisphere dominates the other one. Standard deviation (σ_R) of the reported hemispheric ratio (Table 1) was estimated in accordance with the following formula by *Ku* [1966] (NIST/SEMATECH e-Handbook of Statistical Methods, 2006, available at http://www.itl.nist.gov/div898/handbook/):

$$C_R = \frac{1}{\sqrt{N}} \cdot \frac{X_N}{X_S} \cdot \sqrt{\frac{C_N^2}{X_N^2} + \frac{C_S^2}{X_S^2} - 2 \cdot \frac{C_{NS}^2}{X_N \cdot X_S}}$$

where C_N, C_S are standard deviations of zonal averaged AOTs in the Northern and Southern hemispheres, respectively, C_{NS} is their covariance, and N stands for the number of months in the AOT global monthly data set used (N = 96 for the MISR and MODIS-Terra data sets, N = 60 for the MODIS-Aqua data set). The same approach was used to estimate the hemispheric ratio of FAOT and CF (Table 1).

[15] In order to investigate long-term AOT changes by using the 8-year global monthly data sets of MISR AOT and MODIS-Terra AOT, the global field of 4-year aerosol difference (δAOT) was obtained by using the following expressions:

$$\delta AOT = AOT(05/08) - AOT(00/04)$$

where *AOT* (05/08), and *AOT* (00/04) stand for the global distribution of AOT averaged for the 4-year periods March 2004 to February 2008 and March 2000 to February 2004, respectively. Positive δAOT corresponds to an increased average difference, i.e., greater AOT overall in the second 4 years than in the fist 4 years, while negative δAOT corresponds to a decreased average difference.

3. Results

3.1. Meridional Aerosol Distribution Over the Global Ocean

[16] The baseline components of the satellite-retrieved AOT over the ocean are (1) marine aerosols (sea salt), which are produced by strong winds over the ocean, (2) mineral desert dust, and (3) anthropogenic biomass burning and urban/industrial pollution aerosols [*Kaufman et al.*, 2005a]. The distribution of desert dust and anthropogenic aerosols over the ocean can be explained by aerosol transport from the land to the ocean by the action of winds. This aerosol transport could result in meridional hemispheric aerosol asymmetry over the ocean (Figure 1a): the AOT hemispheric ratio ranges from 1.39 to 1.51, based on MISR, MODIS-Terra, and MODIS-Aqua data (Table 1). There was close similarity between meridional AOT distributions based on data of different sensors. As estimated, the correlation was about 0.96 between MISR and MODIS (both Terra and Aqua), and close to 1, between MODIS-Terra and MODIS-Aqua. The closest agreement between MODIS-Terra and MODIS-Aqua data is not surprising, given the instrument and algorithm similarity [*Mishchenko et al.*, 2007].

[17] It is worth mentioning that a bimodal maximum is observed in the ocean AOT over the Northern Hemisphere (Figure 1a). An explanation for the bimodal maximum is that the aerosol transport from land to ocean is affected by two different circulation regimes in the Northern Hemisphere, over the Atlantic and Pacific Oceans, as discussed further in section 3.2. In the Southern Hemisphere, the minimum of the averaged total AOT is located at 30°S, and in the tropics the averaged total AOT significantly increases northward.

[18] As a whole over the ocean there is similarity between the meridional distribution of FAOT and of AOT, except at latitudes between 30°S and 60°S (Figure 1b). In particular, the meridional distribution of FAOT also displays hemispheric asymmetry. The FAOT hemispheric ratio ranges from 1.34 to 1.74 based on MISR, MODIS-Terra and MODIS-Aqua data (Table 1). In the Southern Hemisphere, a decrease in the meridional distribution of both AOT and FAOT is observed at latitudes between 0° and 30°S. At latitudes from 30°S to 60°S, a noticeable increase in AOT is accompanied by only slight changes in FAOT (Figure 1b), which is corroborated by all three satellites used.

[19] In the Southern Hemisphere, the AOT maximum between 40–60°S (Figure 1a) is probably due to sea-salt aerosol production, because of strong winds associated with

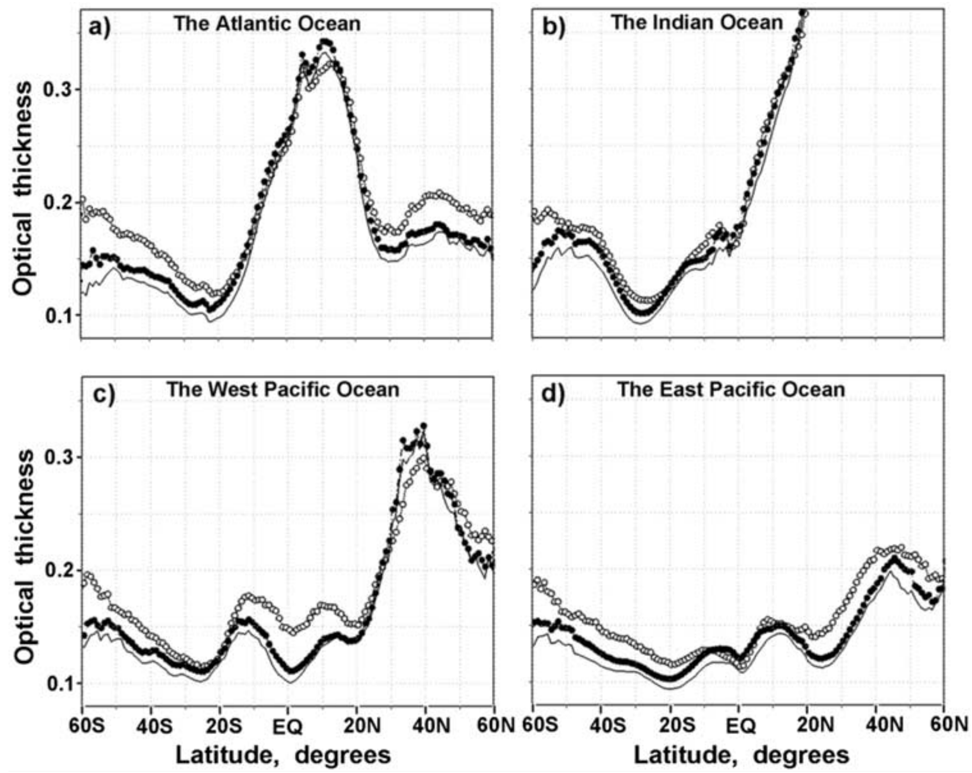

Figure 4. Meridional distributions of ocean AOT, zonal averaged over longitudes (a) 60°W to 0°E in the Atlantic Ocean, (b) 60–120°E in the Indian Ocean, (c) 120–180°E in the West Pacific Ocean, and (d) 180–240°E in the East Pacific Ocean. The designations of AOT from different sensors are the same as in Figure 1.

the "Roaring Forties." At the "Roaring Forties," strong winds, which are not slowed down by any large landmass, could produce aerosols characterized by significant AOT (Figure 1a). This is supported by AVHRR satellite data [*Mishchenko and Geogdzhayev*, 2007], by the Global Aerosol Data Set (GADS) [*Hatzianastassiou et al.*, 2004], by ship-based measurements [*Vinoj et al.*, 2007], and also by numerical simulations of global sea-salt distributions [*Gong et al.*, 2002]. On the other hand, the zone 40–60°S is characterized by high cloud presence exceeding 0.8 (Figure 1c). In accordance with *Remer et al.* [2008], *Zhang et al.* [2005], it is also possible that the increase in AOT could be partially caused by cloud contamination: the aerosol retrievals interpret, in error, cloud droplets as coarse mode particles.

[20] It was found that the meridional distribution of cloud fraction is more symmetrical in both hemispheres than that of AOT (Figure 1c): the CF hemispheric ratio is close to 1 (Table 1). Cloud fraction at low latitudes is lower than at middle latitudes in both hemispheres. In the tropics, a local maximum near the equator was observed, which was surrounded by local minima in the two hemispheres. The local maximum over the equator is probably due to clouds concentrated over the Intertropical Convergence Zone [*Hong et al.*, 2007].

3.2. Bimodal Maximum in Ocean AOT Distributions

[21] A possible explanation of the Northern Hemisphere bimodal maximum is that the aerosol transport from land to ocean is not mainly east-west. Asian aerosols take their route moving in a northeast direction across the Pacific Ocean. This situation contributes to the maximum at 40–50°N. Saharan/Sahelian aerosols are transported southwest from North Africa to South America. That is the reason for the maximum being seen at 10–20°N. It appears as if the land aerosol sources are at 20–40°N, but the aerosol transport from land to ocean is affected by two different circulation regimes in the Northern Hemisphere: predominant westerlies toward the northeast and predominant easterlies to the southwest. Shown in Figure 2, the 8-year mean global distribution of ocean AOT, based on MISR and MODIS-Terra data displays the exact world locations of the local AOT maxima. It can be seen that the two sensors are in agreement with each other on the global distribution of ocean AOT.

[22] Averaged wind distribution over two areas in the Northern Hemisphere, in the Atlantic Ocean (0–40°N; 60°W to 0°E) and in the Pacific Ocean (20–60°N; 120–180°E), was used in the current study to support the aforementioned explanation about the bimodal maximum in the ocean AOT. In particular, NCEP/NCAR reanalysis monthly pressure-level data [*Kalnay et al.*, 1996] were used for spatial and temporal wind averaging. Wind averaging was carried out over the 8-year period under investigation, from March 2000 to February 2008. The wide 700–925 hPa layer is considered as indicative of wind in the lower troposphere, e.g., *Dunion and Velden* [2004] used it to represent the wind within the Saharan Air Layer. Therefore,

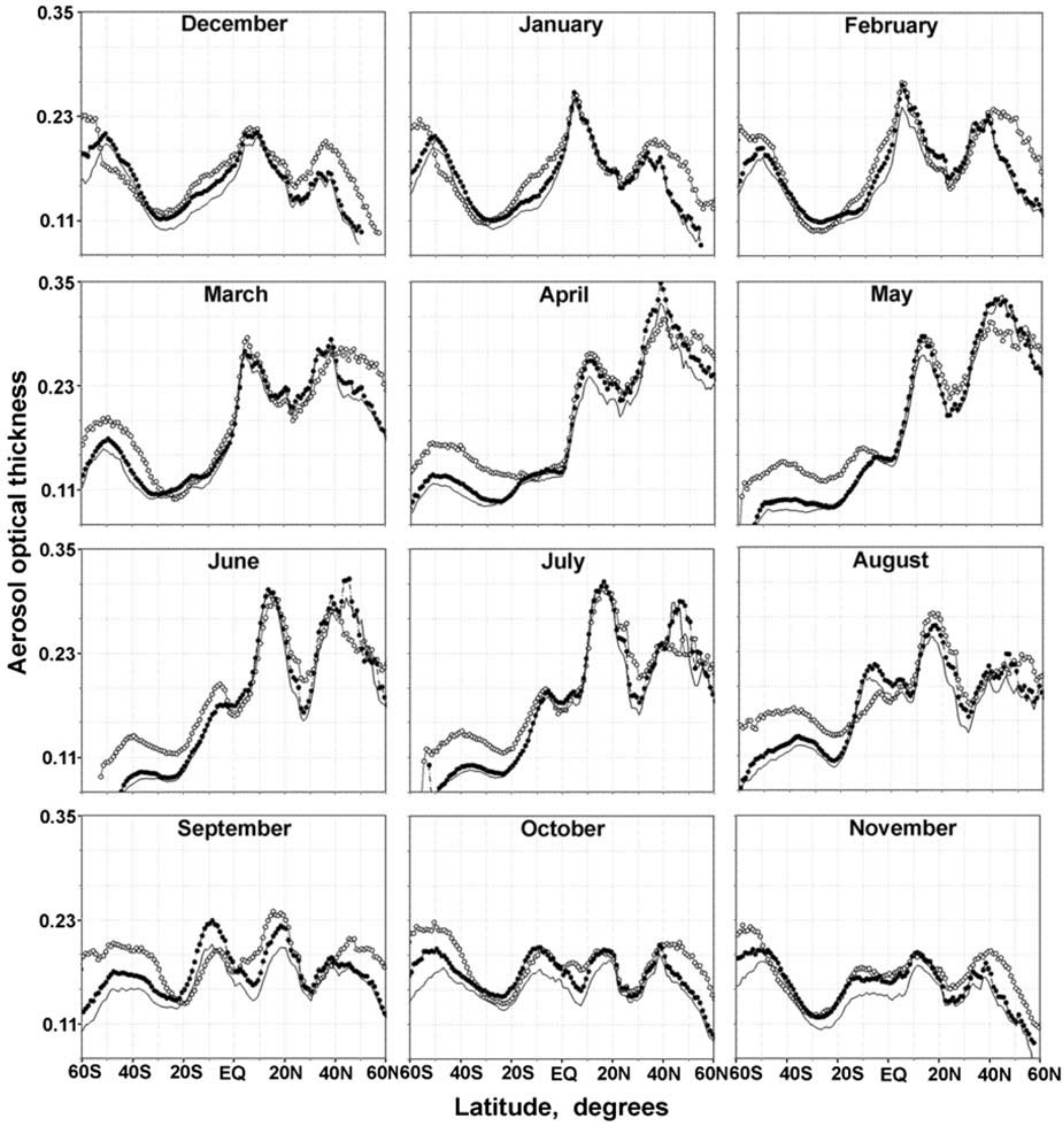

Figure 5. Meridional distribution of zonal averaged total AOT for different months. The designations of AOT from different sensors are the same as in Figure 1.

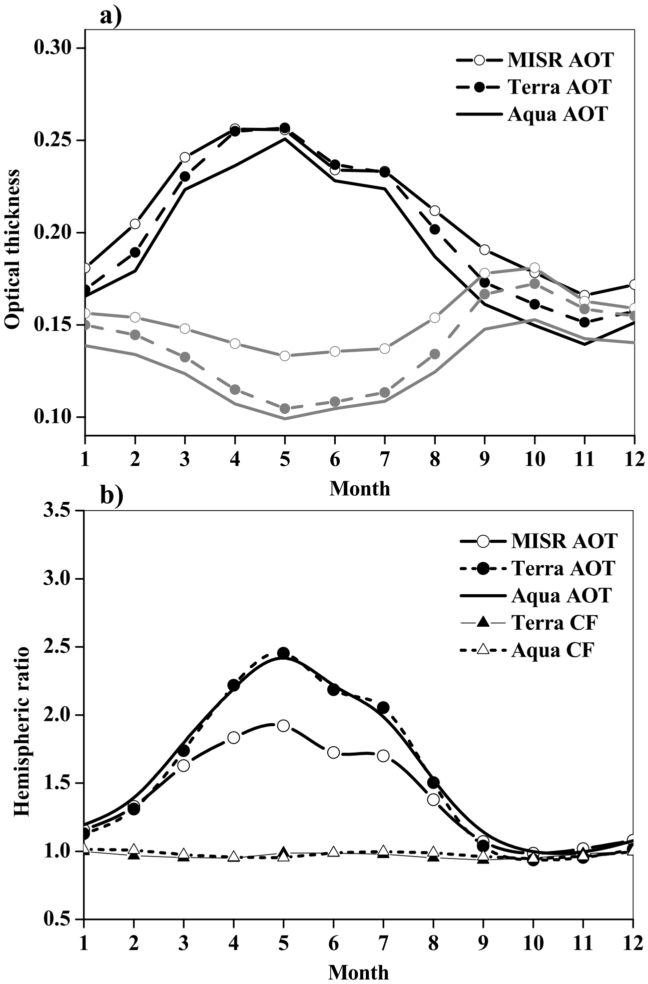

Figure 6. (a) Seasonal variations of AOT averaged over the Northern (black lines) and Southern (gray lines) hemispheres. (b) Seasonal variations of the hemispheric ratio of AOT and cloud fraction. The designations are the same as in Figure 1.

in the current study, in addition to averaging over the 8-year period under investigation, the wind was also averaged from 700 hPa to 925 hPa pressure levels. Mean wind vectors over the aforementioned Atlantic and Pacific areas are displayed in Figures 3a and 3b. It is clearly seen that predominant easterlies over the Atlantic Ocean could transfer Saharan/Sahelian land aerosols in a southwest direction from North Africa (Figure 3a). Therefore, high aerosol concentrations could be produced at latitudes 10–20°N by the action of Atlantic easterly winds. As seen in Figure 3b, over the Pacific Ocean, Asian land aerosols could be transported by Pacific westerly winds in the northeast direction across the Pacific ocean, contributing to the aerosol maximum at 40–50°N.

[23] An analysis of meridional distribution of ocean AOT, separately over the Atlantic, Indian, and Pacific longitude zones helps us understand contributory factors of the bimodal maximum. Figure 4 represents the meridional distribution of ocean AOT, zonally averaged over the Atlantic (60°W to 0°E), the Indian Ocean (60–120°E), the West Pacific Ocean (120–180°E), and the East Pacific Ocean (180–240°E). Over the Atlantic Ocean (Figure 4a), the only monomodal maximum in the AOT distribution is observed at latitudes 10–20°N, in accordance with the predominant circulation regime of easterly winds. Over the West and East parts of the Pacific Ocean (Figures 4c and 4d), the only monomodal maximum in the AOT distribution is observed at latitudes 40–50°N, in accordance with the predominant westerly winds. This fact is direct evidence that two different circulation regimes in the Northern Hemisphere, over the Atlantic and Pacific Oceans, play an important role in the formation of the bimodal maximum in ocean AOT.

[24] Our analysis shows, however, that the aforementioned circulation regimes are not the only reason for the formation of the bimodal maximum. Over the Indian Ocean, a noticeable increase in AOT from the equator up to 20°N was observed (Figure 4b), which could also contribute to high aerosol concentrations at latitudes 10–20°N.

3.3. Seasonal Variations of Meridional Aerosol Distribution

[25] Meridional aerosol distribution was analyzed for each month of the year. As shown in Figure 5, hemispheric aerosol asymmetry does exist but not in every month: the asymmetry is not prominent during the half-year period from September to February. In contrast, from March to August, hemispheric aerosol asymmetry between the two hemispheres is prominent. Moreover, it is most prominent from April to July. As seen in Figure 5, three different sensors, MISR, MODIS-Terra, and MODIS-Aqua, provide quite similar aerosol distributions. In the Northern Hemisphere at latitudes between 0°N and 20°N, during the season of the most prominent asymmetry, meridional aerosol distributions based on data sets of different sensors fairly well coincided.

[26] On the basis of the analysis of seasonal variations of AOT averaged over the Northern Hemisphere and that averaged over the Southern Hemisphere, it was found that seasonal variations of AOT in the Southern Hemisphere are opposite to those in the Northern Hemisphere. As illustrated in Figure 6a, seasonal changes of total AOT, averaged over the Northern Hemisphere, show maximum during the season from March to August and minimum during the season from September to February. In contrast to the Northern Hemisphere, in the Southern Hemisphere, minimum AOT is achieved during the season from March to August, while maximum AOT is achieved from September to February. Accordingly, the hemispheric ratio of AOT reaches its seasonal maximum from March to August, as displayed in Figure 6b, on the basis of the available data sets of MISR, MODIS-Terra and MODIS-Aqua data. Note that all three sensors used showed high negative correlation between seasonal variations of AOT in the Northern and Southern hemispheres: the correlation was estimated to be equal to −0.80, −0.93, and −0.95 for MISR, MODIS-Terra, and MODIS-Aqua, respectively. As the seasonal increase in AOT in the Northern Hemisphere is accompanied by the seasonal decrease in AOT in the Southern Hemisphere, this makes it clear that both the Northern and Southern hemi-

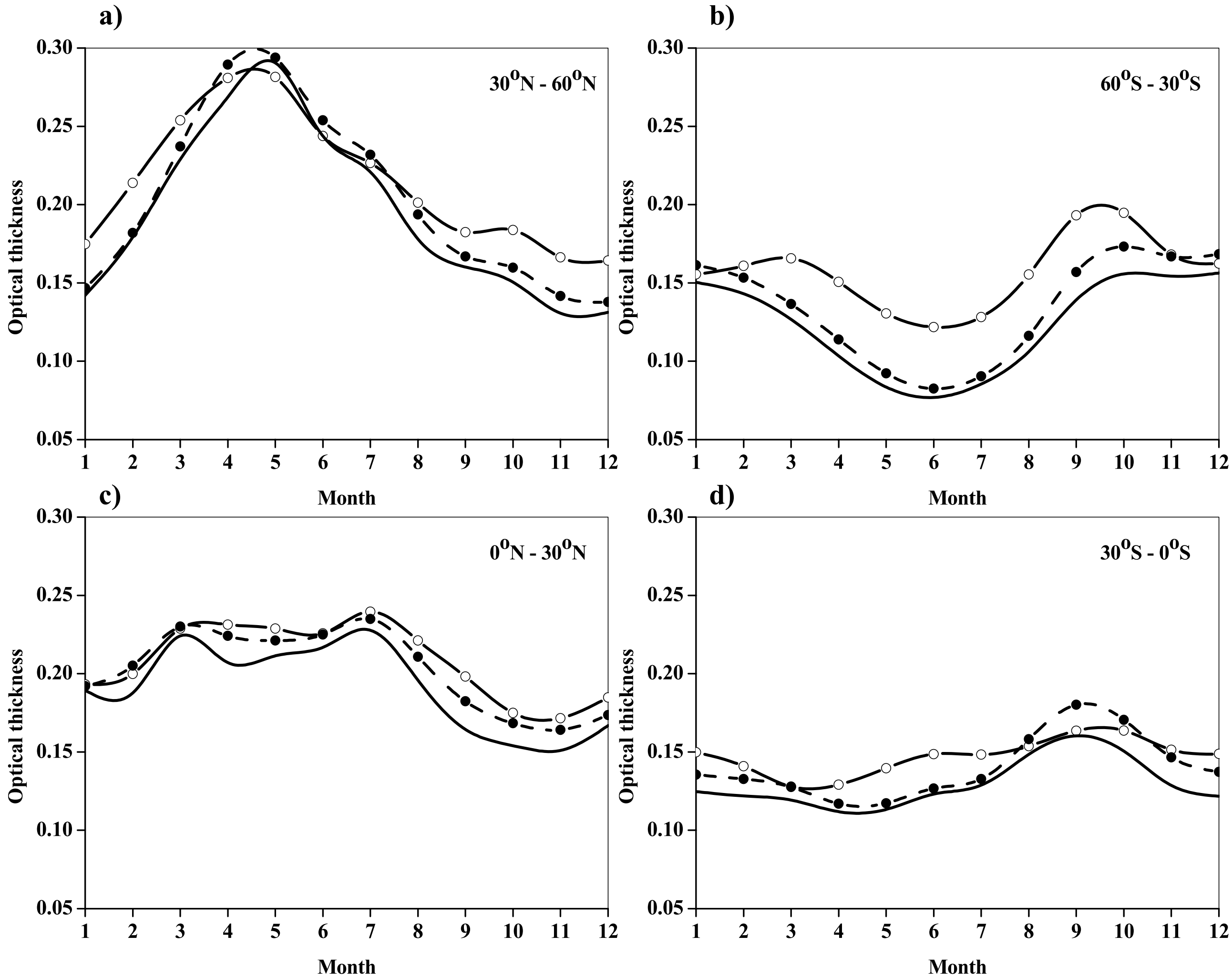

Figure 7. Seasonal variations of AOT averaged over different latitude zones: (a) 60°N to 30°N, (b) 30–60°S, (c) 30°N to 0°, (d) 0–30°S. The designations of AOT from different sensors are the same as in Figure 1.

spheres contribute to the formation of meridional hemispheric aerosol asymmetry.

[27] It is interesting to analyze seasonal variations of zonal averaged AOT within different latitudinal intervals in the Northern and Southern hemispheres. In particular, seasonal variations of zonal averaged AOT were analyzed within the following four 30-degree latitudinal intervals: 30–60°N, 0°N to 30°, 0–30°S, and 30–60°S. As illustrated in Figures 7a and 7c, in both latitudinal zones of the Northern Hemisphere, AOT reaches its maximum values during the half-year period from March to August, while AOT reaches its minimum from September to February. The seasonal variations of AOT at midlatitudes in the Northern Hemisphere (30–60°N) are more pronounced than those at low latitudes (0°N to 30°) (Figures 7a–7c).

[28] Seasonal variations of AOT in the Southern Hemisphere were opposite to those in the Northern Hemisphere at corresponding latitudes: minimum AOT was observed from March to August, while maximum AOT was observed from September to February (Figures 7b–7d). As in the Northern Hemisphere, in the Southern Hemisphere, seasonal variations of AOT were more pronounced at midlatitudes (30–60°S) than at low latitudes (0–30°S) (Figures 7b–7d).

[29] Seasonal variations of averaged AOT separately over the Atlantic (60°W to 0°E) and Pacific (120–240°E) Oceans, in different latitudinal zones of the Northern Hemisphere, were also analyzed (Figure 8). One can see that both over the Atlantic and Pacific zones the three sensors show broadly similar seasonal variations of averaged AOT. At midlatitudes in the Northern Hemisphere (30–60°N), the main contribution to the seasonal variations of AOT over the ocean was made by the Pacific Ocean aerosols (Figures 8c–8d). In contrast to midlatitudes, at low latitudes (0°N to 30°), aerosols over the Atlantic Ocean contribute to seasonal variations of AOT more significantly than aerosols over the Pacific Ocean (Figures 8e–8f).

[30] In accordance with the aforementioned seasonal variations of meridional aerosol distribution, AOT is different over the two hemispheres and is seasonally dependent. This can be illustrated by 8-year mean distributions of total AOT, based on data sets of the two sensors, MISR and MODIS-Terra (Figure 9). It can be seen that the distribution

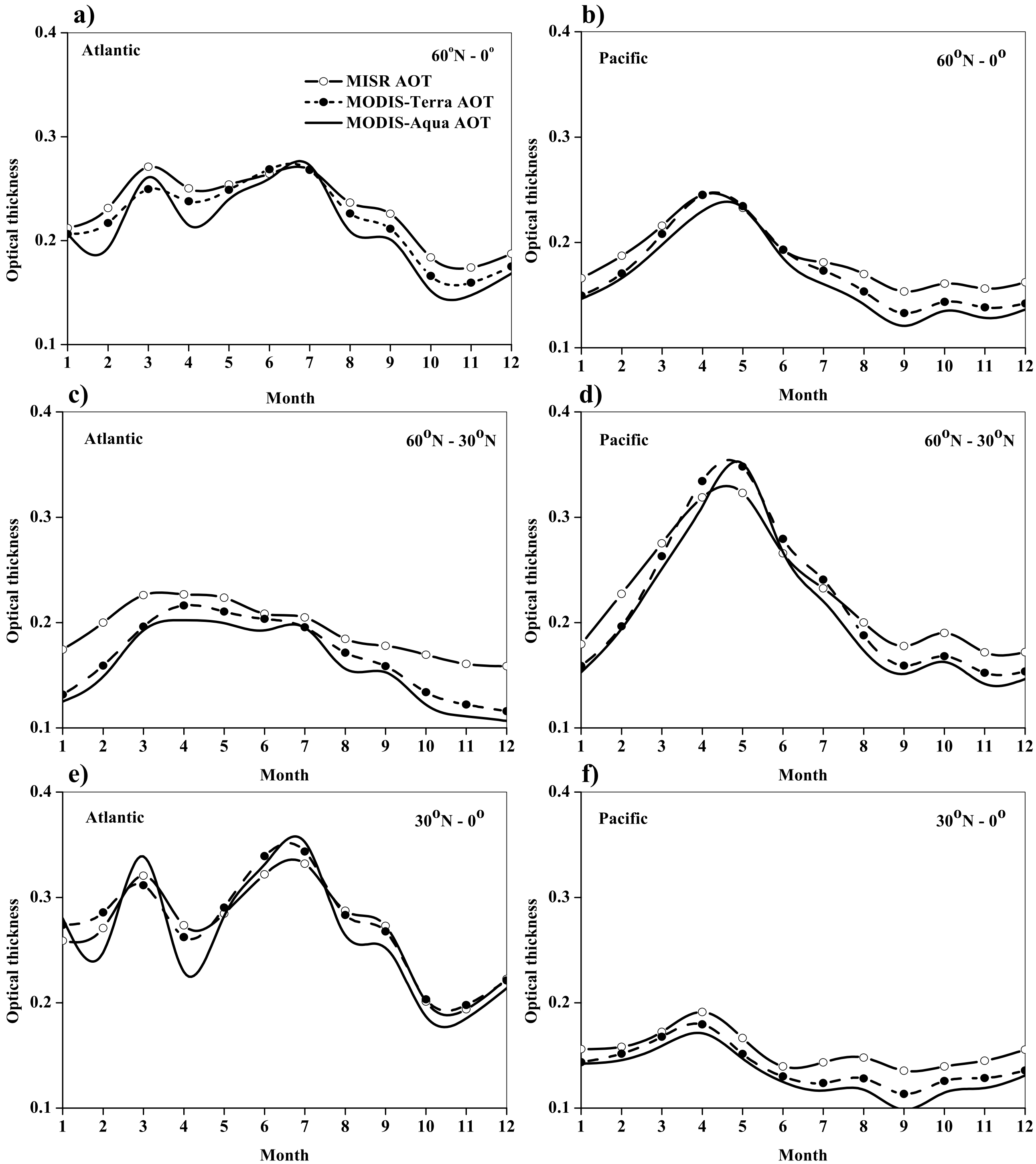

Figure 8. Comparison between seasonal variations of average AOT over the Atlantic Ocean (60°W to 0°E) (left column) and those over the Pacific Ocean (120–240°E) (right column) within different latitudinal zones in the Northern Hemisphere: (a, b) 60°N to 0°, (c, d) 60–30°N, and (e, f) 30°N to 0°. The designations of average AOT from different sensors are the same as in Figure 1.

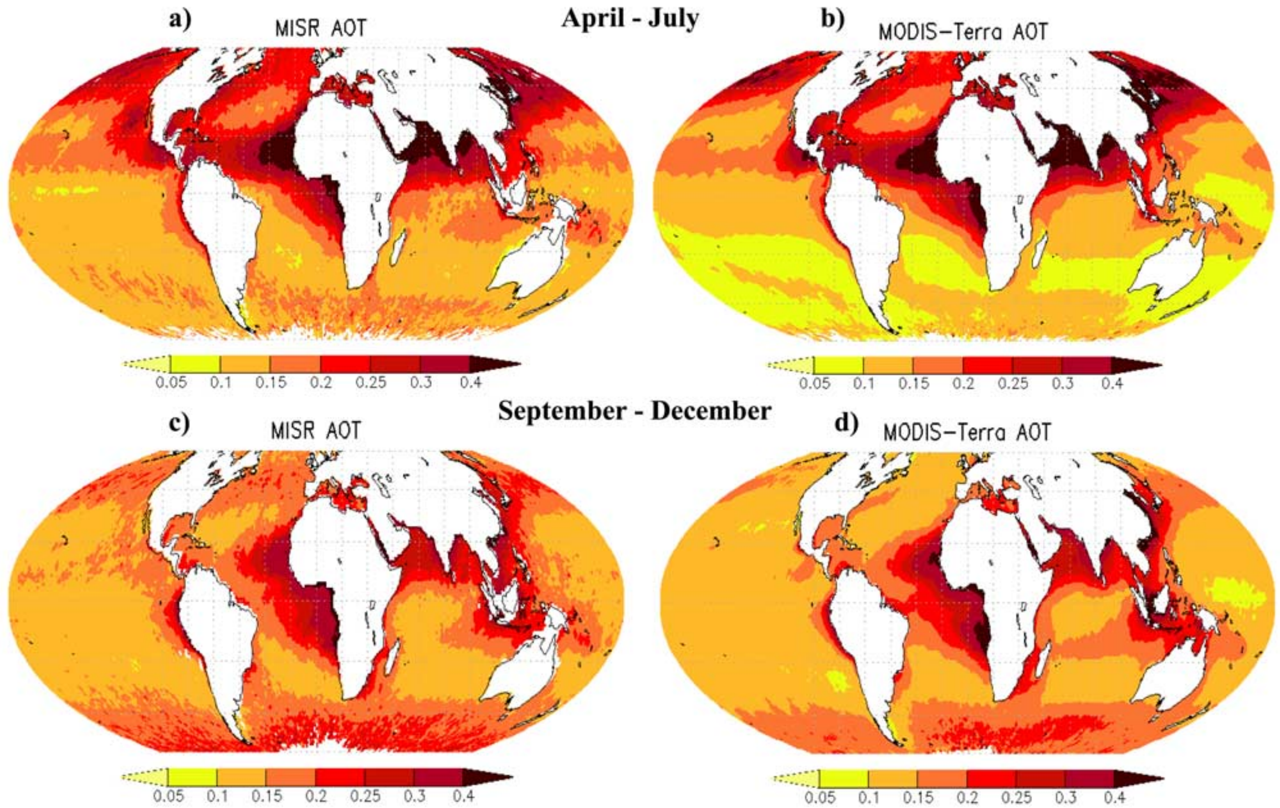

Figure 9. (a, b) The 8-year mean distribution of AOT for the season of the most pronounced meridional aerosol asymmetry, from April to July. (c, d) The 8-year mean distribution of AOT for the season with no noticeable meridional aerosol asymmetry, from September to December. The left column corresponds to MISR AOT while the right column corresponds to MODIS-Terra AOT.

of total AOT for the two sensors is in agreement in the Northern Hemisphere, for the season from April to July (Figures 9a–9b) when meridional aerosol asymmetry is the most pronounced. Note that for the season from September to December, when there is no noticeable meridional aerosol asymmetry, the two sensors are in agreement in the Southern Hemisphere (Figures 9c–9d).

3.4. Long-Term AOT Changes and Solar Dimming-Brightening

[31] It is worth noting that the major industrial zones of Europe and North America are located at midlatitudes between 30°N and 60°N. Furthermore, as discussed in section 3.2, transport of aerosols, both natural and anthropogenic, from China and other countries of southeast Asia, to the region 30–60°N takes place because of the predominant circulation regime over the Pacific Ocean. According to *Christopher et al.* [2006], meridional distribution of estimated direct radiative forcing of anthropogenic aerosols over the cloud-free ocean also shows a maximum between 30°N and 60°N. These three facts suggest that anthropogenic aerosols could contribute to ocean AOT over the region 30–60°N, and thereby they could contribute to the modulation of surface solar radiation in cloudless conditions.

[32] In accordance with *Wild et al.* [2005], during the period from the mid-1980s to 2002, solar brightening was observed over the land, based on the Global Energy Balance Archive (GEBA) database of pyranometer measurements. Using the GEBA database, updated on pyranometer measurements up to the year 2007 (M. Wild, personal communication, 2008), it was found that solar brightening over the land was observed at midlatitudes in the Northern Hemisphere (30–60°N), which is the period under consideration in the current study. Moreover, a 40% decrease in fine particle aerosol optical thickness over Europe, in cloudless conditions for the summer months, was detected by using the 8-year MODIS-Terra aerosol products, from 2000 to 2007 (K. Karnieli et al., Temporal trend in anthropogenic sulfur aerosol transport from central and eastern Europe to Israel, submitted to *Journal of Geophysical Research*, 2008). If aerosols over the ocean reflect the processes with aerosols over the land, then one could expect to find prevailing declining tendencies in AOT over the ocean.

[33] Accurate detection of long-term trends requires several decades of data [*Weatherhead et al.*, 1998], which were not available for the sensors used. Therefore, in the current study, as a first approximation of the overall aerosol tendencies during the 8-year period under consideration, we used 4-year aerosol differences (δAOT and δFAOT) between the last 4 years (March 2004 to February 2008) and the first 4 years (March 2000 to February 2004) (see section 2). A similar approach to estimate long-term aerosol changes, based on AVHRR satellite data, was used by *Mishchenko and Geogdzhayev* [2007]. For completeness, the 8-year time series of AOT and FAOT over the ocean at latitudes between 30°N and 60°N were also analyzed.

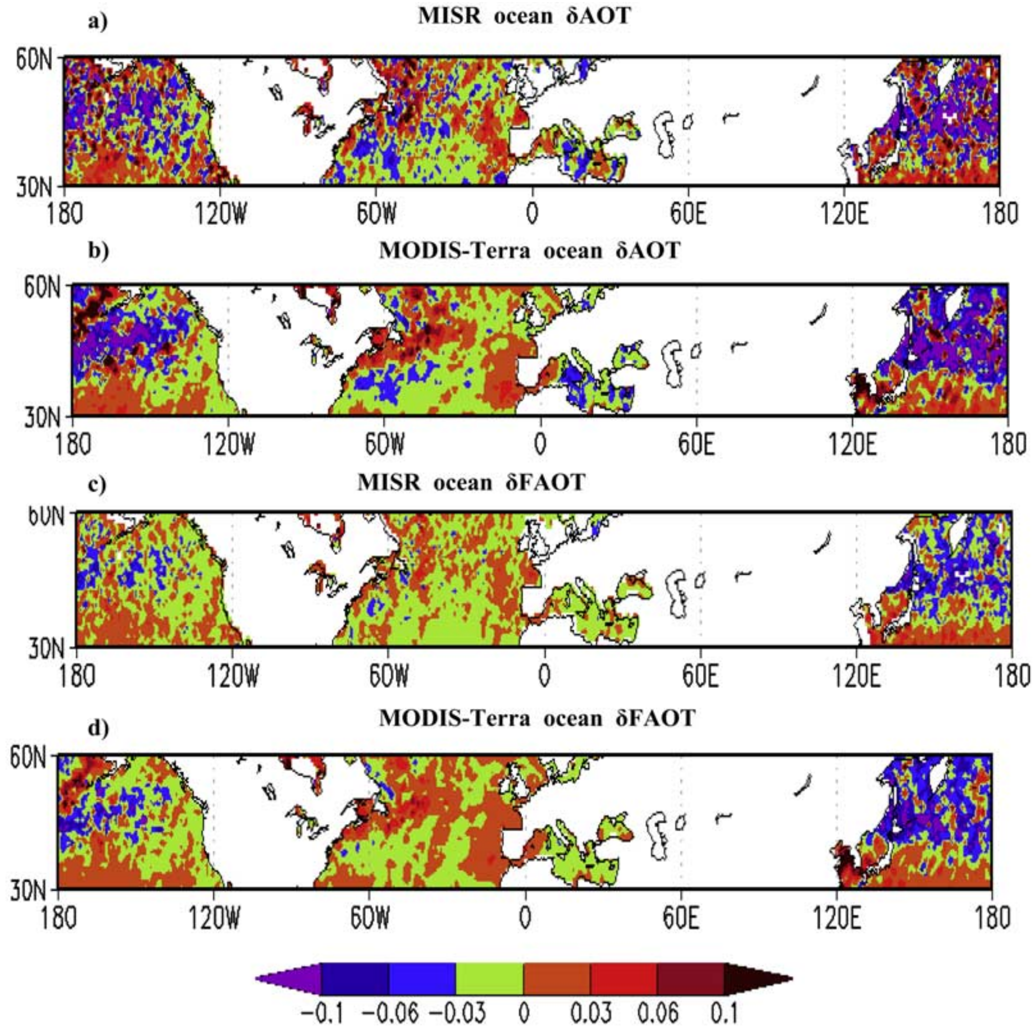

Figure 10. The distribution of 4-year aerosol differences (δAOT/δFAOT) between the last 4 years (March 2004 to February 2008) and the first 4 years (March 2000 to February 2004) at latitudes between 30–60°N for the season of the most pronounced meridional aerosol asymmetry, from April to July: (a, b) δAOT over the ocean (Figure 10a, MISR; Figure 10b, MODIS-Terra) and (c, d) δFAOT over the ocean (Figure 10c, MISR; Figure 10d, MODIS-Terra).

[34] As displayed in Figures 10a–10b (Figures 10c–10d), the distribution of MISR δAOT (δFAOT) for April–July months has certain features in common with that of MODIS-Terra: negative aerosol differences slightly dominate at midlatitudes in the Northern Hemisphere (30–60°N). As estimated in percentage terms, both MISR and MODIS-Terra data show that, over the ocean, the area with observed negative δAOT (δFAOT) was equal to approximately 60% of the total ocean area at latitudes 30–60°N. Averaged 4-year differences $< \delta\text{AOT} >$ and $< \delta\text{FAOT} >$ over the ocean latitudinal zone 30–60°N during the season from April to July are displayed in Table 2, together with their standard deviation. As one might notice, the negative aerosol tendencies appear only slight because $< \delta\text{AOT} >$ and $< \delta\text{FAOT} >$ are small. Moreover, these tendencies are not statistically significant because the values of their standard deviation are large in comparison with the values of $< \delta\text{AOT} >$ and $< \delta\text{FAOT} >$ (Table 2). For same reasons we could not identify any consistent aerosol tendencies during the September–December months (see Table 2).

[35] By analyzing the 8-year time series of ocean AOT (FAOT), we found that there are no statistically significant tendencies in AOT (FAOT) either in April–July, the season of pronounced meridional aerosol asymmetry, or in Septem-

Table 2. Averaged Four-Year Differences[a]

Season	MISR		MODIS-Terra	
	$< \delta\text{AOT} >$	$< \delta\text{FAOT} >$	$< \delta\text{AOT} >$	$< \delta\text{FAOT} >$
April–July	−0.016 ± 0.067	−0.009 ± 0.027	−0.010 ± 0.055	−0.002 ± 0.013
September–December	−0.002 ± 0.038	−0.002 ± 0.014	−0.001 ± 0.023	0.002 ± 0.017

[a] $< \delta\text{AOT} >$ and $< \delta\text{FAOT} >$ (± their standard deviation) over the ocean latitudinal zone 30–60°N during the two seasons: from April to July and from September to December.

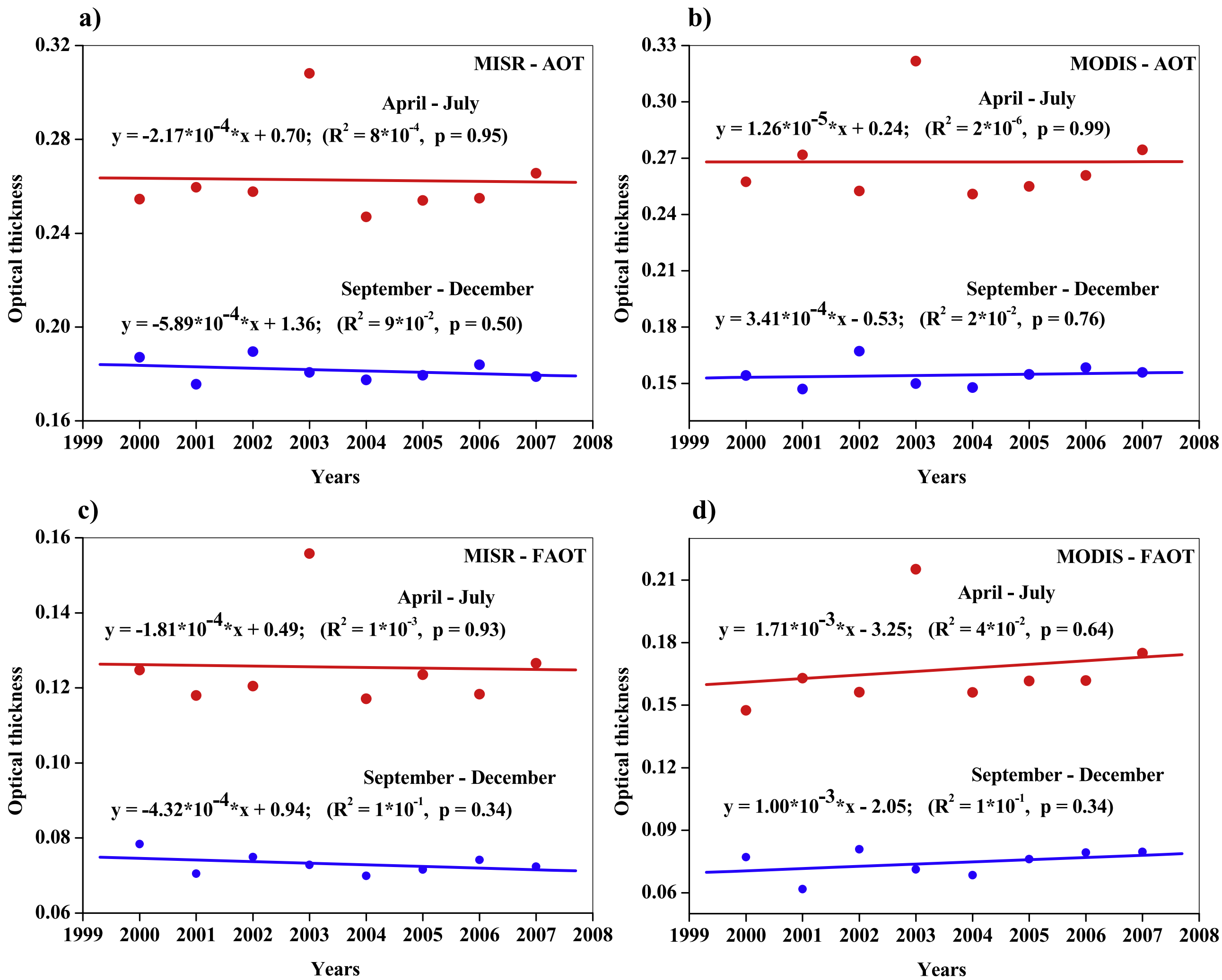

Figure 11. The 8-year time series of (left) MISR and (right) MODIS-Terra aerosol data averaged over the ocean in the latitudinal zone 30–60°N: (a, b) aerosol optical thickness and (c, d) fine aerosol optical thickness. The plotted linear fits are not statistically significant: their measure of estimated linear fit, the coefficient of determination (R^2), is too low. The p value is too high as compared with the 0.05 significance level.

ber–December, the season without noticeable aerosol asymmetry. Shown in Figures 11a–11d, the scattered points do not conform to a linear fit for determining statistically significant tendencies of ocean AOT and FAOT. To be specific, we estimated and plotted the linear fits for all time series of AOT (FAOT) presented in Figures 11a–11d, even though their slopes are not statistically significant. In particular, the measure of estimated linear fit, the coefficient of determination R^2, is too low (Figure 11).

[36] Therefore, one can conclude that, in cloudless condition, solar brightening was not observed over the ocean, at latitudes 30–60°N, during the 8-year period under consideration, 2000–2008. The fact is consistent with our previous findings [*Alpert and Kishcha*, 2008]. On the basis of pyranometer data from the global network, we found that solar dimming was not observed over sparsely populated sites, remote from the main industrial zones. This is even more relevant to remote ocean areas: solar dimming-brightening is not observed there as those areas are thousands of kilometers distant from highly populated and/or industrial zones. Note, however, that the pyranometer data include both cloud and aerosol effects on surface solar radiation. In the current study, long-term aerosol variations were analyzed in cloudless conditions.

4. Discussions and Conclusions

[37] We have used the 8-year MISR and MODIS-Terra data sets, from March 2000 to February 2008, as well as the 5-year MODIS-Aqua data set, from July 2002 to June 2007, in order to analyze meridional distribution of aerosol optical thickness and its tendencies over the ocean. Obtained meridional distributions of aerosol optical thickness were verified by comparing the three sensors: similar results obtained by the three different data sets support each other. Our analysis has led us to the following conclusions:

[38] 1. Over the ocean there is pronounced meridional aerosol asymmetry. It was found that there were seasonal variations in the meridional aerosol asymmetry: it was pronounced during the half-year period, from March to

August (the most pronounced asymmetry was observed from April to July). There was no noticeable meridional hemispheric asymmetry during the season from September to December. We found that not only the Northern Hemisphere but also the Southern Hemisphere contributed to the formation of noticeable meridional aerosol asymmetry. During the season from March to August, the increase in AOT in the Northern Hemisphere was accompanied by a decrease in AOT in the Southern Hemisphere. The main contribution to the seasonal variations of AOT over the ocean at midlatitudes in the Northern Hemisphere (30–60°N) was made by Pacific Ocean aerosols (Figures 8c–8d). In contrast to midlatitudes, at low latitudes (0–30°N), aerosols over the Atlantic Ocean contributed to seasonal variations of AOT more significantly than aerosols over the Pacific Ocean (Figures 8e–8f).

[39] 2. The meridional aerosol asymmetry is a complex phenomenon, which can be caused by different contributory factors. The main sources of natural and anthropogenic aerosols are located in the Northern Hemisphere: these sources include major deserts and industrial sources of anthropogenic emissions. The increase in AOT in the Northern Hemisphere from March to August suggests an increase in aerosol transport from the land to the ocean. In contrast to the Northern Hemisphere, the decrease in AOT in the Southern Hemisphere from March to August suggests a decrease in aerosol transport from the land to the ocean in local fall and winter. The Northern Hemisphere bimodal maximum was observed in the meridional distribution of AOT over the ocean. An explanation for this includes two contributory factors. The first factor is associated with two different circulation regimes in the Northern Hemisphere: predominant westerlies toward the northeast across the Pacific Ocean and predominant easterlies to the southwest across the Atlantic Ocean. Another contributory factor to the bimodal maximum is significant AOT over the Indian Ocean, from the equator up to 20°N.

[40] 3. During the 8-year period under consideration, 2000–2008, solar brightening, detected over the land, was not observed in cloudless conditions over the ocean at midlatitudes (30–60°N) in the Northern Hemisphere. This suggests that the solar dimming-brightening phenomenon is rather a local (regional) one, restricted to highly populated and/or industrial zones.

[41] **Acknowledgments.** We gratefully acknowledge L. Remer, R. Levy, and Y. Agnon for their helpful discussion, the GES-DISC Interactive Online Visualization and Analysis Infrastructure (Giovanni) for providing MODIS data, the NASA Langley Research Center Atmospheric Sciences Data Center for providing MISR data, and NOAA/OAR/ESRL Physical Science Division for providing NCEP reanalysis data from their Web site (http://www.cdc.noaa.gov/). This study was supported by the GLOWA–Jordan River BMBF (Germany)–MOST (Israel) project, the BMBF-MOST grant 1946 on global change, and the Israeli Science Foundation (ISF) grant 764/06. C. N. Long acknowledges the support of the Climate Change Research Division of the U.S. Department of Energy as part of the Atmospheric Radiation Measurement (ARM) Program. The work of O. Kalashnikova is supported by a grant from the NASA Earth Sciences Division, Climate and Radiation program, under H. Maring. The work of O. Kalashnikova was performed at the Jet Propulsion Laboratory, California Institute of Technology, under contract with NASA.

References

Acker, J. G., and G. Leptoukh (2007), Online analysis enhances use of NASA Earth science data, *Eos Trans. AGU*, *88*(2), doi:10.1029/2007EO020003.

Alpert, P., and P. Kishcha (2008), Quantification of the effect of urbanization on solar dimming, *Geophys. Res. Lett.*, *35*, L08801, doi:10.1029/2007GL033012.

Alpert, P., P. Kishcha, Y. Kaufman, and R. Schwarzbard (2005), Global dimming or local dimming?: Effect of urbanization on sunlight availability, *Geophys. Res. Lett.*, *32*, L17802, doi:10.1029/2005GL023320.

Bellouin, N., O. Boucher, J. Haywood, and M. S. Reddy (2005), Global estimate of aerosol direct radiative forcing from satellite measurements, *Nature*, *438*, 1138–1141, doi:10.1038/nature04348.

Chou, M.-D., P.-K. Chan, and M. Wang (2002), Aerosol radiative forcing derived from SeaWIFS-Retrieved aerosol optical properties, *J. Atmos. Sci.*, *59*, 748–757, doi:10.1175/1520-0469(2002)059<0748:ARFDFS>2.0.CO;2.

Christopher, S., and J. Wang (2004), Intercomparison between multi-angle Imaging SpectroRadiometer (MISR) and sunphotometer aerosol optical thickness in dust source regions of China, implications for satellite aerosol retrievals and radiative forcing calculations, *Tellus, Ser. B*, *56*, 451–456, doi:10.1111/j.1600-0889.2004.00120.x.

Christopher, S., J. Zhang, Y. Kaufman, and L. Remer (2006), Satellite-based assessment of top of atmosphere anthropogenic aerosol radiative forcing over cloud-free oceans, *Geophys. Res. Lett.*, *33*, L15816, doi:10.1029/2005GL025535.

Chu, D. A., Y. J. Kaufman, C. Ichoku, L. A. Remer, D. Tanre, and B. N. Holben (2002), Validation of MODIS aerosol optical depth retrieval over land, *Geophys. Res. Lett.*, *29*(12), 8007, doi:10.1029/2001GL013205.

Chu, D. A., et al. (2005), Evaluation of aerosol properties over ocean from Moderate Resolution Imaging Spectroradiometer (MODIS) during ACE-Asia, *J. Geophys. Res.*, *110*, D07308, doi:10.1029/2004JD005208.

Diner, D. J., et al. (1998), Multi-angle Imaging SpectroRadiometer (MISR) instrument description and experiment overview, *IEEE Trans. Geosci. Remote Sens.*, *36*, 1072–1087, doi:10.1109/36.700992.

Dunion, J. P., and C. S. Velden (2004), The impact of the Saharan air layer on Atlantic tropical cyclone activity, *Bull. Am. Meteorol. Soc.*, *85*(3), 353–365, doi:10.1175/BAMS-85-3-353.

Gong, S. L., L. A. Barrie, and M. Lazare (2002), Canadian Aerosol Module (CAM): A size-segregated simulation of atmospheric aerosol processes for climate and air quality models: 2. Global sea-salt aerosol and its budgets, *J. Geophys. Res.*, *107*(D24), 4779, doi:10.1029/2001JD002004.

Hatzianastassiou, N., B. Katsoulis, and I. Vardavas (2004), Sensitivity analysis of aerosol direct radiative forcing in ultraviolet-visible wavelengths and consequences for the heat budget, *Tellus, Ser. B*, *56*(4), 368–381, doi:10.1111/j.1600-0889.2004.00110.x.

Hong, G., B. C. Gao, B. Baum, Y. X. Hu, M. King, and S. Platnik (2007), High cloud properties from three years of MODIS Terra and Aqua collection 4 data over the tropics, *J. Appl. Meteorol. Climatol.*, *46*(11), 1840–1856.

Ichoku, C., L. A. Remer, Y. J. Kaufman, R. Levy, D. A. Chu, D. Tanre, and B. N. Holben (2003), MODIS observation of aerosols and estimation of aerosol radiative forcing over southern Africa during SAFARI 2000, *J. Geophys. Res.*, *108*(D13), 8499, doi:10.1029/2002JD002366.

Jethva, H., S. K. Satheesh, and J. Srinivasan (2007), Assessment of second-generation MODIS aerosol retrieval (collection 005) at Kanpur, India, *Geophys. Res. Lett.*, *34*, L19802, doi:10.1029/2007GL029647.

Kahn, R., B. Gaitley, J. Martonchik, D. Diner, K. Crean, and B. Holben (2005), MISR global aerosol optical depth validation based on two years of coincident AERONET observations, *J. Geophys. Res.*, *110*, D10S04, doi:10.1029/2004JD004706.

Kalashnikova, O. V., and R. Kahn (2009), Mineral dust plume evolution over the Atlantic from MISR and MODIS aerosol retrievals, *J. Geophys. Res.*, *113*, D24204, doi:10.1029/2008JD010083.

Kalnay, E., et al. (1996), The NCEP/NCAR 40-year reanalysis project, *Bull. Am. Meteorol. Soc.*, *77*(3), 437–470, doi:10.1175/1520-0477(1996)077<0437:TNYRP>2.0.CO;2.

Kaufman, Y. I., D. Tanré, and O. Boucher (2002), A satellite view of aerosols in the climate system, *Nature*, *419*, 215–223, doi:10.1038/nature01091.

Kaufman, Y. J., O. Boucher, D. Tanre, M. Chin, L. A. Remer, and T. Takemura (2005a), Aerosol anthropogenic component estimated from satellite data, *Geophys. Res. Lett.*, *32*, L17804, doi:10.1029/2005GL023125.

Kaufman, Y. J., et al. (2005b), A critical examination of the residual cloud contamination and diurnal sampling effects on MODIS estimates of aerosol over ocean, *IEEE Trans. Geosci. Remote Sens.*, *43*(12), 2886–2897, doi:10.1109/TGRS.2005.858430.

King, M. D., W. P. Menzel, Y. J. Kaufman, D. Tanre, B. C. Gao, S. Platnick, S. A. Ackerman, L. A. Remer, R. Pincus, and P. A. Hubanks (2003), Cloud and aerosol properties, precipitable water, and profiles of temperature and humidity from MODIS, *IEEE Trans. Geosci. Remote Sens.*, *41*(2), 442–458, doi:10.1109/TGRS.2002.808226.

Kishcha, P., B. Starobinets, and P. Alpert (2007), Latitudinal variations of cloud and aerosol optical thickness trends based on MODIS satellite data, *Geophys. Res. Lett.*, *34*, L05810, doi:10.1029/2006GL028796.

Kleidman, R. G., N. T. O'Neill, L. A. Remer, Y. J. Kaufman, T. F. Eck, D. Tanre, O. Dubovik, and B. N. Holben (2005), Comparison of Moderate Resolution Imaging Spectroradiometer (MODIS) and Aerosol Robotic Network (AERONET) remote-sensing retrievals of aerosol fine mode fraction over ocean, *J. Geophys. Res.*, *110*, D22205, doi:10.1029/2005JD005760.

Ku, H. (1966), Notes on the use of propagation of error formulas, *J. Res. Natl. Bur. Stand. U. S. Sect. C*, *70*(4), 263–273.

Levy, R. C., L. A. Remer, D. Tanre, Y. J. Kaufman, C. Ichoku, B. N. Holben, J. M. Livingston, P. B. Russell, and H. Maring (2003), Evaluation of the Moderate Resolution Imaging Spectroradiometer (MODIS) retrievals of dust aerosol over the ocean during PRIDE, *J. Geophys. Res.*, *108*(D19), 8594, doi:10.1029/2002JD002460.

Levy, R. C., L. A. Remer, J. V. Martins, Y. J. Kaufman, A. Plana-Fattori, J. Redemann, P. B. Russell, and B. Wenny (2005), Evaluation of the MODIS aerosol retrievals over ocean and land during CLAMS, *J. Atmos. Sci.*, *62*, 974–992, doi:10.1175/JAS3391.1.

Levy, R. C., L. A. Remer, S. Mattoo, E. F. Vermote, and Y. J. Kaufman (2007a), Second-generation algorithm for retrieving aerosol properties over land from MODIS spectral reflectance, *J. Geophys. Res.*, *112*, D13211, doi:10.1029/2006JD007811.

Levy, R. C., L. A. Remer, and O. Dubovik (2007b), Global aerosol optical properties and application to MODIS aerosol retrieval over land, *J. Geophys. Res.*, *112*, D13210, doi:10.1029/2006JD007815.

Liepert, B. (2002), Observed reductions of surface solar radiation at sites in the United States and worldwide from 1961 to 1990, *Geophys. Res. Lett.*, *29*(10), 1421, doi:10.1029/2002GL014910.

Liu, Y., J. A. Sarnat, B. A. Coull, P. Koutrakis, and D. J. Jacob (2004), Validation of Multiangle Imaging Spectroradiometer (MISR) aerosol optical thickness measurements using Aerosol Robotic Network (AERONET) observations over the contiguous United States, *J. Geophys. Res.*, *109*, D06205, doi:10.1029/2003JD003981.

Martonchik, J. V., D. J. Diner, R. Kahn, and B. Gaitley (2004), Comparison of MISR and AERONET aerosol optical depths over desert sites, *Geophys. Res. Lett.*, *31*, L16102, doi:10.1029/2004GL019807.

Mishchenko, M. I., and I. V. Geogdzhayev (2007), Satellite remote sensing reveals regional tropospheric aerosol trends, *Opt. Express*, *15*, 7423–7438, doi:10.1364/OE.15.007423.

Mishchenko, M. I., I. V. Geogdzhayev, B. Cairns, B. E. Carlson, J. Chowdhary, A. A. Lacis, L. Liu, W. B. Rossow, and L. D. Travis (2007), Past, present, and future of global aerosol climatologies derived from satellite observations: A perspective, *J. Quant. Spectrosc. Radiat. Transf.*, *106*, 325–347, doi:10.1016/j.jqsrt.2007.01.007.

Papadimas, C. D., N. Hatzianastassiou, N. Mihalopoulos, X. Querol, and I. Vardavas (2008a), Spatial and temporal variability in aerosol properties over the Mediterranean basin based on 6-year (2000–2006) MODIS data, *J. Geophys. Res.*, *113*, D11205, doi:10.1029/2007JD009189.

Papadimas, C. D., N. Hatzianastassiou, N. Mihalopoulos, M. Kanakidou, B. Katsoulis, and I. Vardavas (2008b), Assessment of the MODIS collections C005 and C004 aerosol optical depth products over the Mediterranean basis, *Atmos. Chem. Phys. Discuss.*, *8*, 16,891–16,916.

Pinker, R. T., B. Zhang, and E. G. Dutton (2005), Do satellites detect trends in surface solar radiation?, *Science*, *308*, 850–854, doi:10.1126/science.1103159.

Ramanathan, V., et al. (2007), Atmospheric brown clouds: Hemispherical and regional variations in long-range transport, absoption, and radiative forcing, *J. Geophys. Res.*, *112*, D22S21, doi:10.1029/2006JD008124.

Remer, L. A., and Y. J. Kaufman (2006), Aerosol direct radiative effect at the top of the atmosphere over cloud free ocean derived from four years of MODIS data, *Atmos. Chem. Phys.*, *6*, 237–253.

Remer, L. A., et al. (2002), Validation of MODIS aerosol retrieval over ocean, *Geophys. Res. Lett.*, *29*(12), 8008, doi:10.1029/2001GL013204.

Remer, L. A., et al. (2005), The MODIS aerosol algorithm, products, and validation, *J. Atmos. Sci.*, *62*, 947–973, doi:10.1175/JAS3385.1.

Remer, L. A., et al. (2008), Global aerosol climatology from the MODIS satellite sensors, *J. Geophys. Res.*, *113*, D14S07, doi:10.1029/2007JD009661.

Romanou, A., B. Liepert, G. A. Schmidt, W. B. Rossow, R. A. Ruedy, and Y. Zhang (2007), 20th century changes in surface solar irradiance in simulations and observations, *Geophys. Res. Lett.*, *34*, L05713, doi:10.1029/2006GL028356.

Stanhill, G., and S. Cohen (2001), Global dimming: A review of the evidence for a widespread and significant reduction in global radiation with discussion of its probable causes and possible agricultural consequences, *Agric. For. Meteorol.*, *107*, 255–278, doi:10.1016/S0168-1923(00)00241-0.

Vinoj, V., A. Anjan, M. Sudhakar, S. K. Satheesh, J. Srinivasan, and K. Krishna Moorthy (2007), Latitudinal variation of aerosol optical depths from northern Arabian Sea to Antarctica, *Geophys. Res. Lett.*, *34*, L10807, doi:10.1029/2007GL029419.

Weatherhead, E. C., et al. (1998), Factors affecting the detection of trends: Statistical considerations and applications to environmental data, *J. Geophys. Res.*, *103*(D14), 17,149–17,161, doi:10.1029/98JD00995.

Wild, M., H. Gilgen, A. Roesch, A. Ohmura, C. Long, E. Dutton, B. Forgan, A. Kallis, V. Russak, and A. Tsvetkov (2005), From dimming to brightening: Decadal changes in solar radiation at Earth's surface, *Science*, *308*, 847–850, doi:10.1126/science.1103215.

Zhang, J., J. S. Reid, and B. N. Holben (2005), An analysis of potential cloud artifacts in MODIS over ocean aerosol thickness products, *Geophys. Res. Lett.*, *32*, L15803, doi:10.1029/2005GL023254.

Zhao, T., I. Laszlo, W. Guo, A. Heidinger, C. Changyong, A. Jelenak, D. Tarpley, and J. Sullivan (2008), Study of long-term trend in aerosol optical thickness observed from operational AVHRR satellite instruments, *J. Geophys. Res.*, *113*, D07201, doi:10.1029/2007JD009061.

P. Alpert, P. Kishcha, and B. Starobinets, Department of Geophysics and Planetary Sciences, Tel Aviv University, 69978 Tel Aviv, Israel. (pavel@cyclone.tau.ac.il)

O. Kalashnikova, Jet Propulsion Laboratory, California Institute of Technology, Pasadena, CA 91109, USA.

C. N. Long, Pacific Northwest National Laboratory, Richland, WA 99352, USA.